arXiv:1010.3858v1 [cond-mat.supr-con] 19 Oct 2010

Ferromagnetic resonance with a magnetic Josephson junction

S. E. Barnes[1], M. Aprili[2], I. Petković[3], and S. Maekawa[4]
[1]*Physics Department, University of Miami, Coral Gables, 33124 FL, USA.* [2]*Laboratoire de Physique des Solides, Bât. 510, Université Paris-Sud, 91405 Orsay Cedex, France.* [3]*Service de Physique de l'Etat Condensé/IRAMIS/DSM (CNRS URA 2464), CEA Saclay, F-91191 Gif-sur-Yvette, France.* [4]*Advanced Science Research Center, Japan Atomic Energy Agency, Tokai, Ibaraki 319-1195, and CREST, Japan Science and Technology Agency, Tokyo 102-0075, Japan.*
(Dated: October 20, 2010)

We show experimentally and theoretically that there is a coupling via the Aharonov–Bohm phase between the order parameter of a ferromagnet and a singlet, *s*-wave, Josephson supercurrent. We have investigated the possibility of measuring the dispersion of such spin waves by varying the magnetic field applied in the plane of the junction and demonstrated the electromagnetic nature of the coupling by the observation of magnetic resonance side-bands to microwave induced Shapiro steps.

Rotation symmetry associated with the O(3) orthogonal group forbids a coupling between a scalar *s*-wave order parameter and the vector order parameter $\vec{M}$ of the ferromagnet. However a Josephson junction [1] defines a plane, the O(3) symmetry is broken, and such a coupling is possible. Here we describe a part of the rich spectroscopic magnetic resonance possibilities that this observation implies. It is possible to perform a "photon free" FMR experiment[2] on about 10^7 Ni atoms, something infeasible with standard FMR techniques.

Interactions in nature reflect certain gauge groups and the associate phases which generate a vector potential $\vec{A}$, called the Berry connection[3]. Interactions via electromagnetic fields generated by the conserved electrical currents reflect the U(1) gauge group and the Aharonov–Bohm (AB) phase[4]. Associated with angular moment is the gauge symmetry SU(2) and the familiar Lie algebra, i.e., the spin commutation rules. The AB is replaced by the spin Berry phase. It is often imagined that magnetic moments might interact with the Josephson current by direct spin-flips, which would involve the spin Berry phase[5]. In this paper it will be shown that quantitatively the interaction between the Josephson current and the order parameter in superconductor/ferromagnet/superconductor (SFS) junctions can be explained in terms of the AB-phase and regular electrodynamics. It will be shown such an experiment measures rather directly the magnet correlation function.

We fabricated Nb/$Pd_{0.9}Ni_{0.1}$/Nb Josephson junctions by *in-situ* angle evaporation through a resist mask and subsequent lift-off. The mask is defined by e-beam lithography on a Polyether Sulphone - PES (500 nm)/Si_3N_4(60 nm)/Polymethyl Methacrylate - PMMA (350 nm) trilayer [6] , and etched in a Reactive Ion Etching (RIE) chamber. The Si_3N_4 is etched 1 minute 30 seconds in SF_6 and the PES in Oxygen plasma for 10 minutes, giving an undercut of 500 nm. The mask fabrication process is schematically presented in Fig. 1a. The Si_3N_4 suspended bridge allows shadow evaporation. A scanning- electron-microscope (SEM) picture of the mask including the suspended bridge is reported in Fig. 1c. The first Nb layer is evaporated at -45 degrees with respect to z axis while the PdNi is evaporated at 45 degrees and the second Nb layer at 47 degrees. The overlap in the y direction defines the junction area. The shadow evaporation is illustrated in the lower drawing array of Fig. 1a. Eight junctions are evaporated on the sample chip. A SEM image of one of the junctions after lift-off is shown in Fig. 1d. The electron-gun evaporation is carried out in ultra-high-vacuum (UHV) with a base pressure lower than 10^{-9} mbar. The two Nb superconducting films are 50 nm thick and the ferromagnetic layer of $Pd_{0.9}Ni_{0.1}$

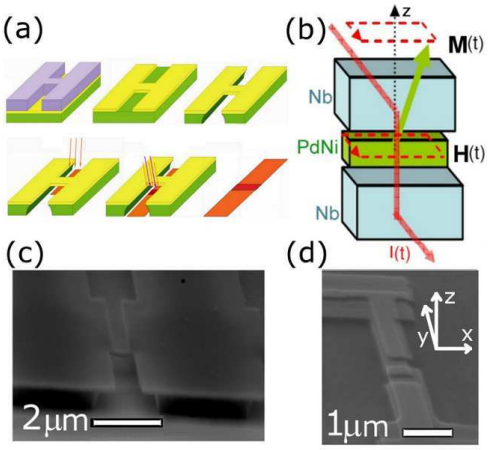

FIG. 1: Description of the sample. **(a)** The fabrication procedure. Trilayer mask is etched to obtain the suspended bridge and the undercut, then the junction is fabricated by shadow evaporation and liftoff. **(b)** The principle of the experiment. AC Josephson current across the junction excites the spin wave modes which in turn couple to the Josephson current and rectification takes place. **(c)** Scanning Electron Microscopy (SEM) picture of the Si_3N_4/PES mask before angle evaporation. **(d)** SEM picture of a junction after lift off.

is 20 nm thick. The Ni concentration is measured by Rutherford Backscattering (RBS) on a test sample. The magnetization loops obtained by SQUID magnetometry with in-plane and out-of-plane magnetic field show a predominant perpendicular anisotropy. Finally, a schematic view of the junction including the principle of the experiment is to be found in Fig. 1b.

Typical current-voltage (IV) characteristics are shown in Fig. 2 as function of temperature. Well below the critical temperature, the critical current $I_c \approx 7\,\mu$A and normal resistance $R_n = 1\,\Omega$ give a Josephson coupling of $7\,\mu$V, consistent with early studies on highly underdamped PdNi-based Josephson junctions [7]. The IV characteristics are not hysteretic confirming overdamped phase dynamics and are well described by the resistively-shunted-junction (RSJ) model [1]. The critical current versus temperature (see inset of Fig. 2) shows the typical linear behavior expected when the Thouless energy of the ferromagnetic layer is larger than the Nb superconducting energy gap. This linear dependence has been observed previously in highly underdamped junctions[7]. The junction critical temperature is about 7.0 K while the critical temperature of the Nb leads is 7.6 K and their critical current over 500 μA at low temperature. We have measured four ferromagnetic junctions on the same wafer, the dispersion of the critical current from junction to junction is about $\pm 1\,\mu$A, ΔR_n is 0.15 Ω while the $I_c R_n$ varies by less than 3% from junction to junction. We have also fabricated non-magnetic junctions by the same process but replacing the PdNi with a thicker 70 nm Pd layer. These junctions have a much larger critical current of about $44\,\mu$A.

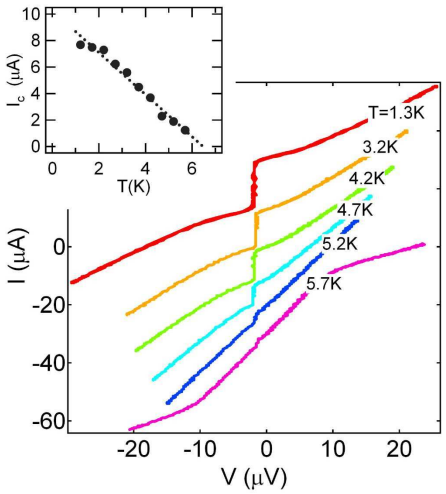

FIG. 2: Current-voltage characteristics with increasing temperature. The curves have been shifted vertically for clarity. They do not show any hysteresis as expected when the phase dynamics is strongly damped. The critical current as a function of the temperature is shown in the insert, the dashed line is a linear fit.

For a square junction of side L, the total super-current is given by the integral [1]

$$I_s = J_c \int_{-L/2}^{L/2} dx \int_{-L/2}^{L/2} dy \sin\phi(x,y,t) \qquad (1)$$

with

$$\phi(\vec{r},t) = \phi_0 + \omega_J t - \frac{2e}{\hbar}\int \vec{A}\cdot d\vec{r}, \qquad (2)$$

where ϕ_0 is an arbitrary phase, $\omega_J = (2e/\hbar)V_0$ is the Josephson frequency, and the last term is the AB phase [8], involving the vector potential $\vec{A}$. We use a gauge where $\vec{A} = A(\vec{r},t)\,\hat{\mathbf{z}}$, the direction $\hat{\mathbf{z}}$ being perpendicular to the junction surface. Therefore $\phi(\vec{r},t) = \phi_0 + kx + \omega_J t - \phi_1$, where ϕ_1 reflects time dependent fields and $k = (4ed/\hbar)\mu_0 H + (4ea/\hbar)\mu_0 M_{0y}$. Here M_{0y} is the y-component of the static magnetisation $\vec{M}_0$, the applied field $\vec{H}$ is in the y direction, $2a$ and $2d = 2(a+\lambda)$ are the actual and magnetic thickness of barrier and λ the London penetration depth. These equations describe both the statics and the dynamics of our junctions.

The approach is similar to that used for junctions with magnetic impurities in a normal metal barrier[9]. It is necessary to determine the appropriate boundary conditions for the solutions of Maxwell's equations. For reasons of transparency, it is not at all useful to solve the very difficult problem in which the solution within the barrier is matched to that in the exterior region to the junction. Within the junction we can ignore the displacement and transport currents since the wavelength of light λ and the skin depth δ are both larger than the dimensions of the junction at the Josephson frequency ω_J relevant for the FMR. We observe that the impedance of the junction of $\sim 1\,\Omega$ is much smaller than 377 Ω of free space and as a consequence there is essentially no radiation from the junction. The displacement current, and evidently, the transport current can therefore also be ignored in the exterior region. It is therefore only necessary to integrate Ampère's circulation law

$$\vec{\nabla}\times\vec{H} = J_s(\vec{r},t)\hat{\mathbf{z}}; \quad J_s = J_c\sin\phi(\vec{r},t) \qquad (3)$$

where ϕ_0 is absorbed by a time translation, and $\phi(\vec{r},t) = kx + \omega_J t - \phi_1$. Required is the additional AB phase shift

$$\phi_1 = \frac{2e}{\hbar}\int_{\vec{r}}^{\vec{r}+2a\hat{\mathbf{z}}} \vec{A}^1\cdot d\vec{r} = \frac{4ae}{\hbar}A_z^1, \qquad (4)$$

with the magnetic system reflected in $\vec{A}^1$. In linear response ϕ_1 is considered as a perturbation and the dc signal is

$$I_1 = -\frac{4ae}{\hbar\omega_J}\frac{1}{T}\int_0^T dt\int_{-L/2}^{L/2} dx\int_{-L/2}^{L/2} dy\frac{\partial J_s}{\partial t}A_z^1 \qquad (5)$$

which includes a time average over a single period T. The determination of $\vec{A}^1$ requires first the vector integration of $\vec{\nabla} \times \vec{H} = J_s(\vec{r},t)\hat{\mathbf{z}}$ and then $\vec{\nabla} \times \vec{A} = \vec{B}$ with $\vec{B} = \mu_0(\vec{H}+\vec{M})$. Even with the simplifications of the previous paragraph, this is an involved calculation. It is useful to make some formal manipulations in order to avoid this double integration. First I_1 is written as

$$I_1 = -\frac{4ae}{\hbar\omega_J}\frac{1}{T}\int_0^T dt \int_{-L/2}^{L/2} dx \int_{-L/2}^{L/2} dy \left(\frac{\partial}{\partial t}\vec{\nabla} \times \vec{H}\right) \cdot \vec{A} \tag{6}$$

using Ampère's law $\vec{J} = \vec{\nabla} \times \vec{H}$. Performing an integration by parts on time we have

$$I_1 = \frac{4ae}{\hbar\omega_J}\frac{1}{T}\int_0^T dt \int_{-L/2}^{L/2} dx \int_{-L/2}^{L/2} dy \left(\vec{\nabla} \times \vec{H}\right) \cdot \frac{\partial \vec{A}}{\partial t}. \tag{7}$$

Using the fact that the Poynting vector, and hence $\vec{H} \times \partial\vec{A}/\partial t = 0$ on the surface, this is integrated again by parts using $\vec{\nabla} \cdot (\vec{H} \times (\partial\vec{A}/\partial t)) = (\partial\vec{A}/\partial t) \cdot \vec{\nabla} \times \vec{H} - \vec{H} \cdot \vec{\nabla} \times (\partial\vec{A}/\partial t)$, to give

$$I_1 = \frac{4ae}{\hbar\omega_J}\frac{1}{T}\int_0^T \int_{-L/2}^{L/2} dx \int_{-L/2}^{L/2} dy \vec{H} \cdot \frac{\partial}{\partial t}\vec{\nabla} \times \vec{A}. \tag{8}$$

Then, since $\vec{\nabla} \times \vec{A} = \vec{B}$ and $\vec{B} = \mu_0(\vec{H} + \vec{M})$, the signal

$$I_1 = -\frac{1}{V_0}\int dv \overline{\vec{H} \cdot \frac{\partial \vec{M}}{\partial t}} \tag{9}$$

where $dv = 2adxdy$ is the elementary volume, the integral is over the volume of the magnetic layer, and the average is indicated by the bar. The resonance of the ferromagnetic layer is contained in $\chi_i(t)$, the dynamic susceptibility, and

$$M_i(\vec{r},t) = \int d\vec{r}' \int dt' \chi_i(\vec{r}-\vec{r}';t-t')H_i(\vec{r}',t'), \tag{10}$$

where $i = x, y, z$. The simple expressions Eqs. (9) and (10) are a principal theoretical result presented here and have an obvious interpretation in terms of the magnetic energy. They demonstrate that Josephson junction magnetic spectroscopy measures very directly the magnetic susceptibility correlation function $\chi_i(\vec{r}-\vec{r}';t-t')$, and all the other excitations to which that couples, in much the same manner as does neutron scattering. As will be seen below, the advantage is that this technique couples preferentially to small q wave vectors.

Since $H_i(\vec{r},t')$ is periodic in time, the *time* convolution Eq. (10), reduces to a product and *if* the susceptibility is sufficiently local and then

$$M_i(\vec{r},\omega_J) = (\chi_i'(\omega_J) + i\chi_i''(\omega_J))H_i(\vec{r},\omega_J) \tag{11}$$

in the usual complex notion. If rather the response is non- local then

$$M_i(\vec{k},\omega_J) = (\chi_i'(\vec{k},\omega_J) + i\chi_i''(\vec{k},\omega_J))H_i(\vec{k},\omega_J) \tag{12}$$

and it requires a Fourier expansion of the spatially dependent $H_i(\vec{r},\omega_J)$. Finally, when $\omega_J \approx I_cR$, as for the lowest voltage experimental signals, the linear response approximation is not strictly applicable and high harmonics of ω_J must be accounted for. Similar expressions apply but now, in particular, "half-harmonic" signals occur since the super-current contains *higher harmonics* and can, corresponding to the second harmonic, excite a resonance at ω_s when $\omega_J/2 = \omega_s$.

Now *all* that is required is a *single* integration of

$$\vec{\nabla} \times \vec{H} = J_c \sin[kx + \omega_J t]\hat{\mathbf{z}}, \tag{13}$$

but which is not a simple task. It is trivial to verify by differentiation that such an integral is $\vec{H}_p = -(J_c/k)\cos(kx + \omega_J t)\hat{\mathbf{y}}$. However this does not satisfy the boundary condition that the current density is zero outside the square junction region. With the present gauge $\vec{A} = A_z\hat{\mathbf{z}}$, it is necessary to find a solution of Laplace's equation $\nabla^2 A_z = 0$ such that $\vec{H} = \vec{H}_p + \vec{H}_i$ where $\vec{H}_i = \vec{\nabla} \times \vec{A}$ is such that $\vec{H}$ satisfies Eq. (13) inside the square but has $\vec{\nabla} \times \vec{H} = 0$ outside. A little reflection suggests there are two contributions to $\vec{H}_i$ which must be accounted for. First, in general, reflecting the even part $J_c \cos kx \sin\omega_J t$ of the current density there is a net oscillating super-current $I_c(H)$ which causes a *circulating* magnetic field about $\hat{\mathbf{z}}$, and second, associated with the spatially odd part of $J_c \sin[kx + \omega_J t]$, there is a uniform component of the field in the $\hat{\mathbf{y}}$-direction. The first contribution is determined by considering the problem with $k = 0$, i.e., with a uniform current density $\overline{J}_s$. The solution is $\vec{H}_s = \frac{1}{2}\overline{J}_s(x\hat{\mathbf{y}} - y\hat{\mathbf{x}})\cos\omega_J t + \ldots$ where the ellipsis reflects the relatively small corrections for a square as compared with a circular cross section. In what follows this correction is ignored. The corresponding vector potential has $A_z = (1/4)\overline{J}_s(x^2 + y^2)$. For finite H, integrating the even part of the current density gives an average super-current density of $\overline{J}_s = J_c \sin(kL/2)/(kL/2)$. By inspection it is observed $A_z = (1/4)\overline{J}_s(-x^2 + y^2)$ satisfies $\nabla^2 A_z = 0$. The corresponding odd $\vec{H}_i^o = x\hat{\mathbf{y}} - y\hat{\mathbf{x}})\cos\omega_J t + \ldots$. The sum $\vec{H}_p + \vec{H}_i^o$ correctly reduces to $\vec{H}_s$ in the limit $k \to 0$. It is the case that $\vec{H}_p$ (and $\vec{H}_p + \vec{H}_i^s$) implies a uniform oscillating field but one which diverges as $k \to 0$, whereas physically, the even part of $\vec{H}_p$ should be proportional to k reflecting the Josephson screening of fields. That the tangential applied field H be continuous requires the current, induced

by the even part of $\vec{H}$, to be zero at the surface. The even part of $\vec{H}_p$ is $-J_c\frac{\cos kx}{k}\sin\omega_J t\hat{\mathbf{y}}(\cos kx/k)\sin\omega_J t\hat{\mathbf{y}}$ The required even part of H_i is now $\vec{H}_i^e = J_c\frac{\cos k\frac{L}{2}}{k}\sin\omega_J t\hat{\mathbf{y}}(\cos k\frac{L}{2}/k)\sin\omega_J t\hat{\mathbf{y}}$, which is equally divergent as $k\to 0$. The net result of integrating Eq. (13) is therefore

$$\vec{H} = \frac{J_c}{k}[\cos(kx+\omega_J t) - \cos\frac{kL}{2}\sin\omega_J t]\hat{\mathbf{y}}$$

$$+\frac{1}{2}J_c\frac{\sin\frac{kL}{2}}{\frac{kL}{2}}(-x\hat{\mathbf{y}} - y\hat{\mathbf{x}})\cos\omega_J t + \ldots \qquad (14)$$

Imagine that the magnetic layer is composed of a number of independent crystallites so that the response is local and Eq. (11) would apply. This local assumption also has the merit of being an useful illustration of the theory since it leads to a relatively simple prediction of the H dependence of the signal which can be compared with experiment. This helps determine if the response is indeed local, or extended. There are some complicated integrals involved in the evaluation of Eq. (9). The result is written, in closed form, as

$$I_m = 2\pi I_c(0)\frac{\Phi_{\rm rf}}{\Phi_0}\left[F_x\chi_x''(\omega_J) + F_y\chi_y''(\omega_J)\right], \qquad (15)$$

where $\Phi_{\rm rf} = (2aL)B_{\rm rf} = (2aL)\mu_0 I_c(0)/L$ is the flux due to the radio frequency field and where

$$F_x = \frac{1}{48}\left[\frac{I_c(B_0)}{I_c}\right]^2$$

and

$$F_y = \frac{2}{x^2}\{1 - \frac{1}{x}\sin\frac{x}{2}\cos\frac{x}{2} - [\frac{11}{24} + \frac{2}{x^2}]\sin^2\frac{x}{2}\},$$

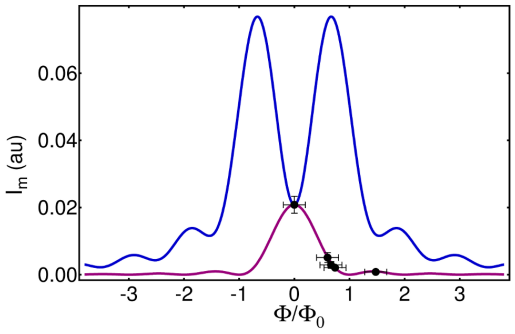

FIG. 3: In blue is F_y and in pink F_x. These curves satisfy the evident requirement that the coefficient of the x and y responses be the same when $B = 0$. Markers denote the experimental values of the resonance amplitude as function of the applied field, with the normalization constant as the fitting parameter.

with $x = kL$, reflect the geometrical structure of the coupling. The equilibrium magnetization is along the z axis, and the magnetic resonance signal is contained in $\chi_x''(\omega_J)$ and $\chi_y''(\omega_J)$, the Fourier transforms of the imaginary part of the susceptibility. The two functions F_x and F_y are plotted in Fig. 3. As required by symmetry $F_x = F_y$ when $k = 0$. The $\chi_x''(\omega_J)$ response near the first zero in $I_c(B_0) = I_c$ is about four times the maximum response to $\chi_y''(\omega_J)$. While there is a clear reflection of the Fraunhofer diffraction pattern in the $\chi_y''(\omega_J)$ response, the $1/k^2$, i.e., $1/H^2$ response dominates that to $\chi_x''(\omega_J)$ with only modulations due to diffraction effects. With a single flux quantum threading thorough the junction the F_x is zero reflecting the net absence of a circulating current. In contrast F_y is a maximum since the current is odd and the junction constitutes a small flat solenoid carrying the critical current density and hence a maximum field internal to the junction.

Given a static magnetisation $\vec{M} = M_z\hat{\mathbf{z}}$ the magnetic susceptibility might be approximated by

$$\chi_x''(\vec{k},\omega) = \chi_y''(\vec{k},\omega) \approx \gamma_e M_z \sum_{\pm}\frac{(\frac{1}{\tau})}{(\omega_s + ak^2 \mp \omega)^2} \qquad (16)$$

where τ is the relaxation time, ω_s the frequency of the FMR mode and a the spin-wave stiffness. Here $\gamma_e = \mu_B/\hbar$ with μ_B the Bohr magneton.

In Fig. 4 we report the dynamical conductance at zero applied magnetic field (solid line) and the theoretical expectation (dotted line) from Eq. (15) and (16) with $a = 0$, using ω_s and $1/\tau$ as a parameters. We obtained ω_s=23 μV as expected from the Kittel's formula $\omega_s = \gamma_e\sqrt{(H_K - 4\pi M_S)^2 - H^2}$, where the anisotropy field H_K and saturation magnetisation M_S have been measured separately by SQUID magnetometry [2]. The FMR frequency is consistent with the value obtained in a reference sample by EPR spectroscopy [2], i.e., the observed signals are entirely consistent with the coupling of the FMR resonance to the superconductivity via the AB-phase. The resonance at 11.5 μV is a subharmonic of the main mode. Kittel's formula predicts that ω_s decreases with increasing H whereas the half-harmonic signal of Fig. 4 actually seems to increase (see inset of Fig. 4). This leads us to believe that this signal corresponds to a finite value of a and k in Eq. (16). That the spin-wave dispersion might be measured in our type of experiment is an exciting possibility warranting further investigation. Moreover, in Fig. 3 we also report the amplitude of the FMR signal (markers) as a function of the applied magnetic field. The experimental data follow the F_x coupling function obtained above.

The electromagnetic nature of the response can be confirmed by a study of Shapiro steps[1, 10]. In the absence of a magnetic resonance mode, an applied radio frequency field gives rise to such steps. In order to account for these we write for the bias voltage across the junction

$$V = V_0 + v\cos\Omega t$$

where v and Ω are the amplitude and frequency of the applied microwave field while the constant V_0, as usual, corresponds to a Josephson frequency $\omega_J = 2eV_0/\hbar$. The Josephson current is now J_c times

$$\sin[kx + \omega t + \frac{2ev}{\hbar\Omega}\sin\Omega t].$$

Expanding this sine with the Jacobi-Anger identity gives

$$\left[J_0(\frac{2ev}{\hbar\Omega})S_0 + \sum_{n=1}^{\infty}\left(J_{2n}(\frac{2ev}{\hbar\Omega})S_{2n} + J_{2n-1}(\frac{2ev}{\hbar\Omega})S_{2n-1}\right)\right]$$

with $S_{2n} = \sum_{\pm}\sin(kz + \omega_0 t + 2n\Omega t)$ and $S_{2n-1} = \sum_{\pm}\pm\sin(kx \pm \omega_0 t + (2n-1)\Omega t)$, where $S_0 = S_{2n=0}$. Each term is of the form

$$J_c^n \sin[kz + \omega_0 t \pm n\Omega t] \rightarrow J_c^n \sin[kz + \omega^n t] \qquad (17)$$

where, in well known fashion[1], $J_c^n = J_c J_n(2ev/\hbar\Omega)$ involves the appropriate Bessel function $J_n(2ev/\hbar\Omega)$. For the voltage at which $\omega^n = 0$ there is a direct contribution $J_c^n \sin(\phi_0 + kx)$ to the average current which is equivalent to the zero voltage critical current step but displaced to $V_n = n\hbar\Omega/2e$ and reduced from $I_c(H)$ to $I_c(H)J_n(2ev/\hbar\Omega)$. This corresponds to the principal Shapiro steps, shown on the top panel of Fig. 5. For the magnetic response, in the linear response regime, the theory developed without an applied microwave field can be adopted. All that is needed is to replace J_c by J_c^n and ω_J with ω^n in the appropriate places as described above.

We have investigated the Shapiro steps for different microwave power. The top part of Fig. 5 shows the appearance of the Shapiro steps in the current-bias characteristics for increasing microwave power. The amplitude of each step follows the appropriate Bessel function $J_n(2ev/\hbar\Omega)$, as expected. In the bottom panel of Fig. 5 is presented the dependence of the magnetization induced side-bands on the micro-wave power. To make these bands more evident, shown is the dynamical resistance as a function of the voltage. It is clear from the data that the amplitude of the side-band resonances follows the Bessel function of the Shapiro steps, as expected from the theory described above. Indeed the Shapiro steps can be seen as "replica" of the critical current at finite bias and hence the side-band amplitude follows that of the steps. The two sidebands correspond to the two poles of the dynamical susceptibility, Eq. (16).

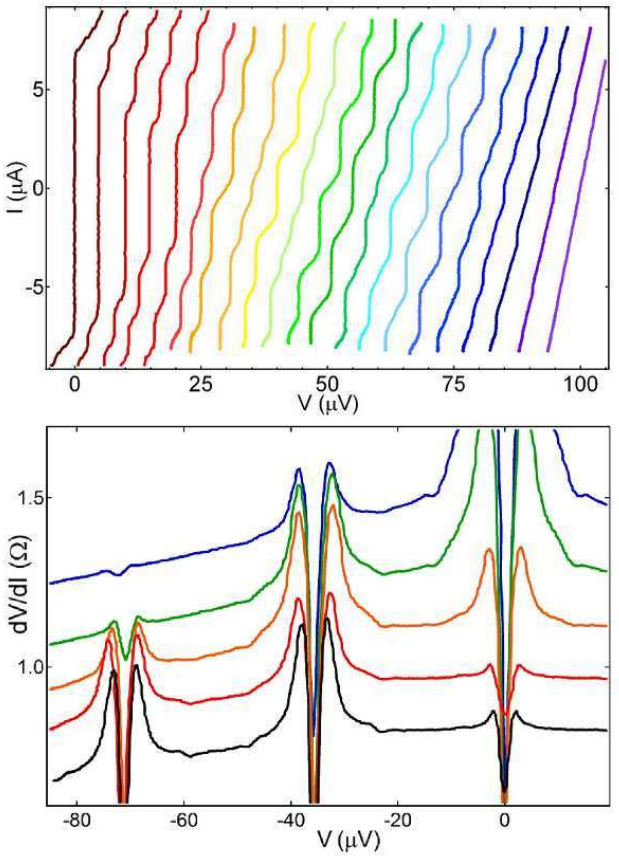

FIG. 5: Top panel: IV curves showing the Shapiro steps, taken at T=1.3 K and with the microwave frequency of 1 GHz with different incident power. Bottom panel: the dynamical resistance showing Shapiro steps and side-band resonances, taken at T=35 mK and with microwave frequency of 17.35 GHz. In passing from the bottom to top the power increases from 0 dBm to 20 dBm, in steps of 5 dBm.

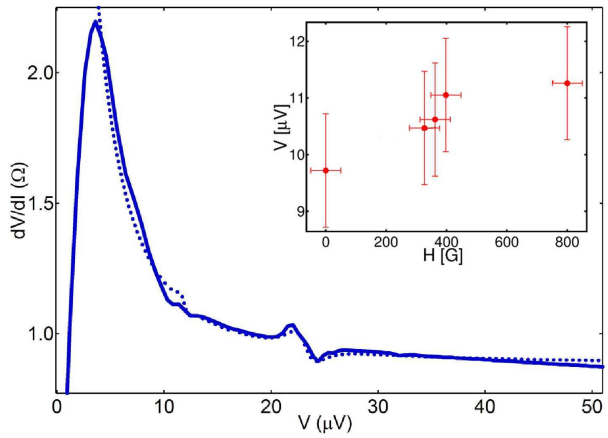

FIG. 4: Dynamical resistance of a ferromagnetic Josephson junction showing ferromagnetic resonances with first and second harmonic. Insert: the magnetic field dependence of the resonance at the second harmonic. The fit takes into account the spatial dispersion of the spin wave mode, see text.

In conclusion, we have described experiments and developed theory to demonstrate that the relative AB phase of the superconductors which comprise a Josephson junction couples to the magnetic order parameter of a ferromagnet. We have thereby performed an FMR experiment with a sensitivity which greatly exceeds that of conventional cavity FMR. Since the coupling is via the magnetic field it is not necessary to have the current pass through

the magnetic material. It might be imagined that the magnetic layer be the top layer of a FSIS structure in which the adjacent S-layer has a thickness of the order of, or less than, the London penetration length. The possibility of measuring the dispersion of spin-wave excitations has also be investigated. Our method[2, 9, 11] of coupling superconductivity to magnetism measures directly the dynamic susceptibility $\chi''(\vec{q},\omega)$ with an enhanced sensitivity for small wave-vectors, complementary to neutron scattering.

[1] See e.g., Barone, A. and Paterno, G. *Physics and Applications of the Josephson Effect* (John Wiley & Sons, New York, 1982).

[2] I. Petković, et al, Phys. Rev. B **80**, 220502(R) (2009).

[3] M. V. Berry Proc. R. Soc. Lond. A **392** 45?57 (1984).

[4] Y. Aharonov, D. Bohm, Phys. Rev. **115** 485?491 (1959).

[5] Z. Nussinov, A. Shnirman, D. P. Arovas, A. V. Balatsky, and J.-X. Zhu, Phys. Rev. B **71**, 214520 (2005); J.-X. Zhu, Z. Nussinov, A. Shnirman, and A. V. Balatsky, Phys. Rev. Lett. **92**, 107001 (2004).

[6] P. Dubos, H. Courtois, B. Pannetier, F. K. Wilhelm, A. D. Zaikin A. D., and G. Schon, Phys. Rev. B **63**, 064502 (2001).

[7] T. Kontos et al. Phys. Rev. Lett. **81**, 301 (2001)

[8] P. W. Anderson, and J. M. Rowell, Phys. Rev. Lett. **10**, 230 (1963).

[9] K. Baberschke, K. D. Bures, and S. E. Barnes, Phys. Rev. Lett. **53**, 98 1984; S. E. Barnes and F. Mehran, Phys. Rev. B **34**, 4537 1986.

[10] S. Shapiro, Phys. Rev. Lett. **11**, 80 (1963).

[11] S.E. Barnes, J.L. Cohn, F. Zuo, Phys. Rev. Lett. **77**, 3252 (1996)